P. G. Charalambides

J. Lund

A. G. Evans

R. M. McMeeking
Mem. ASME

Materials Department,
College of Engineering,
University of California,
Santa Barbara, CA 93106

A Test Specimen for Determining the Fracture Resistance of Bimaterial Interfaces

A test specimen capable of measuring the fracture resistance of bimaterial interfaces has been devised. A finite element approach has been used to characterize trends in the stress intensities and center point displacement with specimen dimensions, elastic properties, and crack length. The utility of the specimen has been demonstrated by conducting experiments on the model system, Al/PMMA.

1 Introduction

Fracture at interfaces between dissimilar materials is a critical phenomenon in many multimaterial systems, ranging from composites (Rühle, Dalgleish, and Evans, 1987) to microelectronic devices (Hsueh and Evans, 1985). Yet, both the fundamental mechanics of this process and experimental techniques capable of systematically characterizing such fracture are incompletely developed. The principal intent of the present article concerns the development of a test procedure for purposes of systematic measurement of the interface fracture resistance.

Most of the important interface fracture problems involve combinations of normal and shear displacements along the crack, such that "mixed mode" conditions prevail. Typical problems include the debonding of fibers in composites (Rühle et al., 1987; Evans et al., 1987) and the decohesion of thin films (Drory, Thouless, and Evans, 1988). Emphasis is placed on a method capable of exploring the associated fracture locus.

An appropriate specimen is depicted in Fig. 1, consisting of a notched, bimaterial flexural beam. It will be demonstrated that this specimen provides fracture results for conditions of approximately equal normal and shear displacements on the interface crack far from the tip but in the K-dominated region. Consequently, when used in conjunction with other specimens, fracture resistance data could be obtained for the range of "mixed mode" space that has direct relevance to the aforementioned fracture problems.

The development of the test specimen involves analytical and finite element solutions of strain energy release rates and stress intensity factors, as well as experimental studies on a model system, consisting of Al bonded to PMMA. Comparisons between theory and experiment allow calibration of the technique and the development of experimental procedures for measuring the fracture resistance.

Contributed by the Applied Mechanics Division for publication in the JOURNAL OF APPLIED MECHANICS.

Discussion on this paper should be addressed to the Editorial Department, ASME, United Engineering Center, 345 East 47th Street, New York, N.Y. 10017, and will be accepted until two months after final publication of the paper itself in the JOURNAL OF APPLIED MECHANICS. Manuscript received by ASME Applied Mechanics Division, August 27, 1987; final revision, April 6, 1988.

2 The Mechanics of Interface Cracks

The small stain elasticity solution in the crack tip region (Fig. 2) can be developed using a bimaterial constant ϵ, which for plane strain is defined following Rice and Sih (1965) and Rice (1988) as

$$\epsilon=(1/2\pi)\ln\{[(3-4\nu_1)/G_1+1/G_2]\,[(3-4\nu_2)/G_2+1/G_1]^{-1}\} \tag{1}$$

where G and ν are the shear modulus and Poisson's ratio, respectively, and the subscripts 1 and 2 refer to the two bonded materials. The relative plane strain displacements of two points on the top and bottom crack surfaces, Δu_x and Δu_y (Fig. 2*a*) can then be expressed in terms of a complex stress intensity factor, K, as (Rice, 1988);

$$\Delta u_y+i\Delta u_x=\frac{2[(1-\nu_1)/G_1+(1-\nu_2)/G_2]K\sqrt{r/2\pi}r^{i\epsilon}}{(1+2i\epsilon)\cosh(\pi\epsilon)} \tag{2}$$

with r being the distance from the crack tip. In general, K can be expressed in terms of its real, Re, and imaginary, Im, parts, through the modulus $|K|$ and the phase angle, ψ,

$$K=|K|e^{i\psi} \tag{3}$$

The physical dimensions of K, as well as its behavior under change of either dimensions or absolute scale, and the ambiguous relationship between the real and imaginary parts of K, have been reviewed recently by Rice (1988). The crack surface displacements can also be written as,

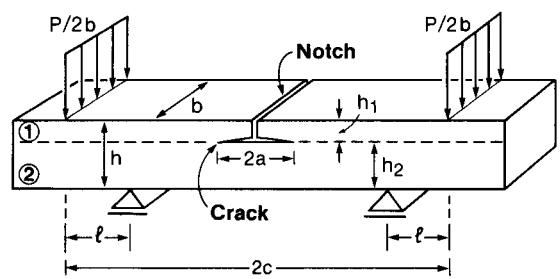

Fig. 1 A bimaterial, notched four-point bending specimen with symmetrical interfacial cracks

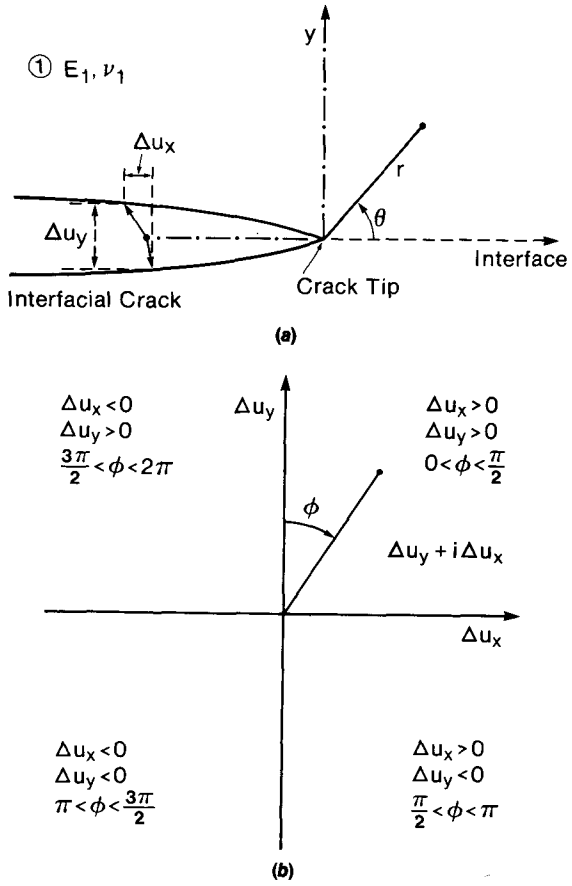

Fig. 2 *(a)* **The crack tip region for an interfacial macrocrack;** *(b)* **The rules for the phase angle ϕ in terms of Δu_x and Δu_y**

$$\Delta u_y + i\Delta u_x = [(\Delta u_x)^2 + (\Delta u_y)^2]^{1/2} e^{i\phi} \tag{4}$$

where ϕ is the phase angle depicted in Fig. 2(*b*). From equations (2) and (4)

$$[(\Delta u_x)^2 + (\Delta u_y)^2]^{1/2} e^{i\omega} = [q|K| r^{1/2} e^{i(\psi-\beta)}]/\sqrt{1+4\epsilon^2} \tag{5}$$

where

$$\beta = \text{Arc tan } (2\epsilon), \text{ and } \omega = \phi - \epsilon \ln r$$

and

$$q = \sqrt{2}\,[(1-\nu_1)/G_1 + (1-\nu_2)/G_2]/\sqrt{\pi}\,\cosh(\pi\epsilon).$$

Consequently, $|K|$ can be expressed in terms of the crack surface displacements as

$$|K| = [(1+4\epsilon^2)(\Delta u_x^2 + \Delta u_y^2)/r]^{1/2}/q \tag{6a}$$

and the phase angle becomes,

$$\psi = \omega + \beta. \tag{6b}$$

The modulus of K can also be related to the plane strain energy release rate $\mathcal{G}$ (Kanninen and Popelar, 1985), by

$$\mathcal{G} = [(1-\nu_1)/G_1 + (1-\nu_2)/G_2]\bar{K}K/4\cosh^2(\pi\epsilon) \tag{7}$$

Furthermore, since $K\bar{K} \equiv |K|^2$

$$|K| = \{4\cosh^2(\pi\epsilon)\mathcal{G}/[(1-\nu_1)/G_1 + (1-\nu_2)/G_2]\}^{1/2}. \tag{8}$$

The preceding results can be used in the following sequence to obtain the requisite interface crack quantities from numerical solutions. First, $\mathcal{G}$ can be explicitly determined either from a contour integral (Rice, 1968) or by a virtual crack extension procedure (Parks, 1974, 1978). The modulus $|K|$ can then be obtained directly from equation (8). Subsequently, the near tip crack surface displacement can be used to obtain an independent estimate of $|K|$, based on equation (6). A comparison provides an internal consistency check, as discussed elsewhere (Matos et al., 1988). Thereafter, the crack surface displacements can be fitted to equation (4), knowing ϵ, to obtain ω. Finally, the results can be expressed in terms of stress intensities

$$\text{Re}(K) = |K| \cos(\omega+\beta) \tag{9a}$$

$$\text{Im}(K) = |K| \sin(\omega+\beta). \tag{9b}$$

3 Analysis of the Specimen

The specimen (Fig. 1) consists of a bimaterial beam. A central notch exists through the thickness of the top layer and a symmetrical precrack is induced along the interface. The specimen is then loaded in four-point flexure. This situation constitutes a well-defined boundary value problem. The solution can be obtained numerically. In addition, an analytical estimate of the energy release rate can be obtained for cracks located between the inner loading points. For purpose of analysis, the subscript 1 indicates quantities relevant to the top layer, whereas the subscript 2 denotes the corresponding quantities for the bottom layer.

3.1 Analytical Solution for the Energy Release Rate. For the crack located between the inner loading lines, the cracked ligament is subject to constant moment conditions. Consequently, by analogy with other decohesion problems, (Drory et al., 1988; Thouless et al., 1987) the strain energy release rate should exhibit steady-state characteristics, at least when the interface crack length significantly exceeds the thickness of the upper layer of the beam. Furthermore, the steady-state value, $\mathcal{G}_{ss}$, can be deduced analytically by recognizing that it is simply the difference in the strain energy in the uncracked and cracked beam. Since there is negligible strain energy in the beam above the crack, $\mathcal{G}_{ss}$ can be deduced from consideration of the energies in the uncracked section, and in a section of the lower beam beneath the crack. From Euler-Bernoulli beam theory and plane strain conditions, these energies can be expressed in terms of the applied moment M as

$$U = (1-\nu^2)\,M^2/2EI \tag{9}$$

where U is the strain energy per unit cross-section and I is the second moment of area per unit width. Consequently,

$$\mathcal{G}_{ss} = \frac{M^2\,(1-\nu_2^2)}{2E_2}\left(\frac{1}{I_2} - \frac{\lambda}{I_c}\right) \tag{10}$$

where

$$\lambda = E_2(1-\nu_1^2)/E_1(1-\nu_2^2)$$

and the subscript c refers to the composite beam. Noting that the moment per unit width $M = Pl/2b$, with P being the total load and l the spacing between inner and outer load lines (Fig. 1),

$$I_c = h_1^3/12 + \lambda h_2^3/12 + \lambda h_1 h_2\,(h_1+h_2)^2/4(h_1+\lambda h_2) \tag{11}$$

and

$$I_2 = h_2^3/12.$$

All dimensions are shown in Fig. 1. The strain energy release rate thus becomes,

$$E_2\mathcal{G}_{ss}h^3b^2/P^2l^2\,(1-\nu_2^2) = (3/2)\,\{1/(h_2/h)^3 - \lambda/\{(h_1/h)^3 + \lambda(h_2/h)^3 + 3\lambda(h_1h_2/h^2)\,[h_1/h + \lambda h_2/h]^{-1}\}\}. \tag{12}$$

Trends in $\mathcal{G}_{ss}$ with relative dimensions h_1/h_2 and relative modulus, E_1/E_2 are depicted in Fig. 3. Evidently, the nondimensional $\mathcal{G}_{ss}$ increases monotonically with increase in relative upper beam thickness, h_1/h_2 and decreases as the relative modulus of the lower layer E_2/E_1, increases.

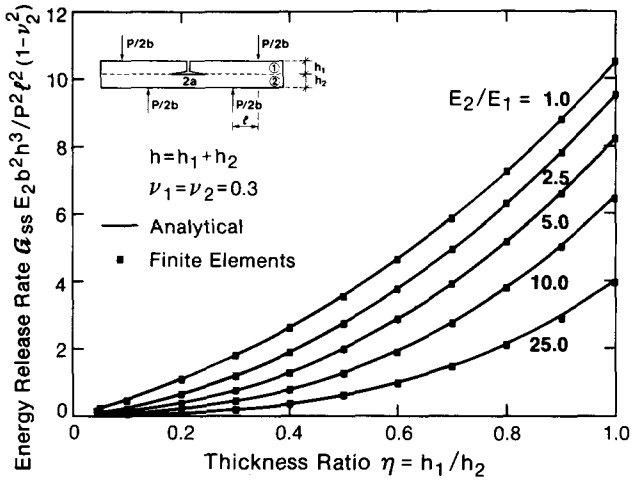

Fig. 3 The trends in the *steady-state* energy release rate with the thickness ratio h_1/h_2, and the modulus ratio E_2/E_1: comparison between analytical and finite element results

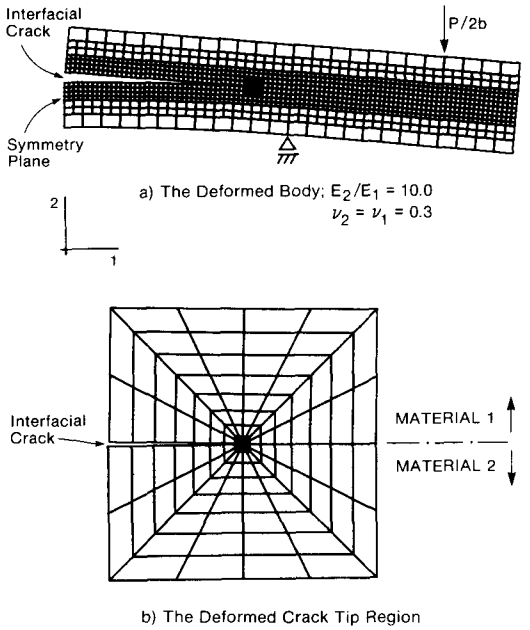

Fig. 4 (*a*) The mesh and the boundary conditions used in the finite element calculations; (*b*) the deformed finite element mesh in the near tip region

3.2 Numerical Solutions.

3.2.1 The Finite Element Procedure. Symmetry about the midsection of the beam depicted in Fig. 1 allows the requisite solutions to be obtained by considering one half of the beam (Fig. 4(*a*)). The finite elements[1] were 8-noded and isoparametric, with four stations used for integration of the stiffness matrix. The number of elements and nodes varied with the relative thickness, h_1/h_2, and with the dimensionless crack length a/l, such that a self-similar focused mesh was generated in the crack tip area having elements small enough to capture the features of the elastic crack tip solution (viz. $\sim h_1/100$ as shown in Fig. 4(*b*)). A roller support fixed the vertical displacement of the inner loading line, whereas symmetry was enforced by inhibiting horizontal displacements along the midsection of the lower layer. The crack surfaces were traction-free.

As noted in Section 2 the modulus of K can be calculated either from the displacement vector $\Delta u_y + i\Delta u_x$ at position r behind the crack tip or from the energy release rate $\mathcal{G}$, using the stiffness derivative method (Parks, 1974, 1978; Matos et al., 1988). The accuracy of $|K|$ computed using displacement magnitudes is subject to the numerical error introduced to the nodal displacements in the crack tip region. This error can be substantial for the first ring of elements around the crack tip. However, the two estimates for $|K|$ agree at a distance r_c from the crack tip (r_c/h is typically 10^{-2} to 10^{-3}) such that nodal displacements in the neighborhood of this region provide a good estimate of K and of the phase angle ψ (Matos et al., 1988). The $|K|$ and ψ estimates reported in this work were extracted from the finite element results, using both the displacement ratios determined at r_c and the energy approach (Matos et al., 1988). The results obtained via the two methods are in excellent agreement (maximum deviation less than 1 percent).

3.2.2 Fracture Mechanics Solutions. Elastic finite element solutions were obtained from various moduli ratios E_2/E_1 and for Poisson's ratios $\nu_1 = \nu_2 = 0.3$ The corresponding Dundurs' parameters α and β (Dundurs, 1969) are presented in Table 1. Elastically deformed meshes (Fig. 4) indicate that the top layer above the crack, being essentially stress-free, experiences rigid body motion determined by the deformation of the beam near the crack tip. Also, the upper beam experiences both opening and sliding relative to the lower beam, indicative of "mixed mode" conditions.

[1]Solved using the ABAQUS finite element program.

Table 1 The plain strain Dundurs' parameters α and β for materials combinations considered in the finite element calculations

Poisson's Ratio		Elastic Modulus Ratio,	Dundurs' Parameters	
ν_1	ν_2	E_2/E_1	α	β
0.3	0.3	1.0	0.0	0.0
0.3	0.3	2.5	- 0.429	- 0.122
0.3	0.3	5.0	- 0.667	- 0.190
0.3	0.3	10.0	- 0.818	- 0.234
0.3	0.3	25.0	- 0.923	- 0.264

$$\alpha = \frac{\frac{G_1}{G_2}(1-\nu_2)-(1-\nu_1)}{\frac{G_1}{G_2}(1-\nu_2)+(1-\nu_1)} \qquad \beta = \frac{1}{2}\frac{\frac{G_1}{G_2}(1-2\nu_2)-(1-2\nu_1)}{\frac{G_1}{G_2}(1-\nu_2)+(1-\nu_1)}$$

The general trends in energy release rate, stress intensity factor and phase angle with crack length are shown in Fig. 5. The mechanics of the bimaterial crack problem (treated in the manner of Rice and Sih (1965)) make it necessary and desirable to normalize K by a typical specimen dimension, such as the full beam depth, $h = h_1 + h_2$. Furthermore, the normalization must include this dimension, raised to the power $i\epsilon$, to allow an unambiguous presentation of the phase relationship between the real and imaginary parts of K. (In the case, $E_2 = E_1$ and $\nu_2 = \nu_1$, $\epsilon = 0$ and $h^{i\epsilon} = 1$). These issues have been reviewed recently by Rice (1988). As expected, the energy release rate $\mathcal{G}$ and the stress intensity factor K attain an essentially constant, steady-state level within a distance from the

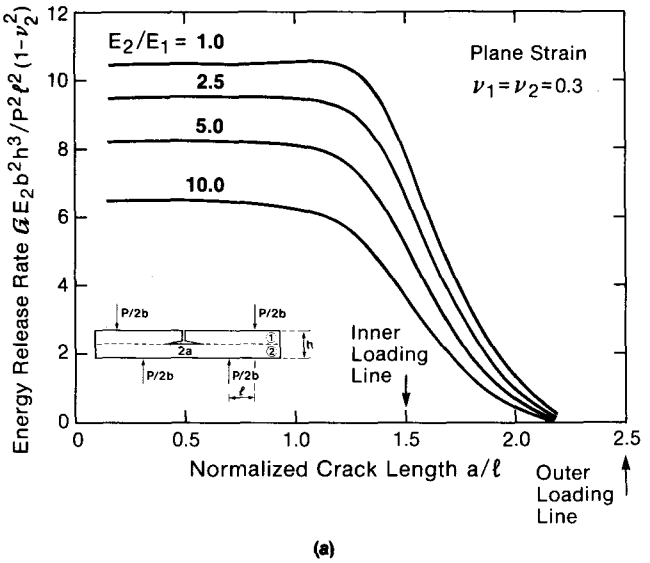

(a)

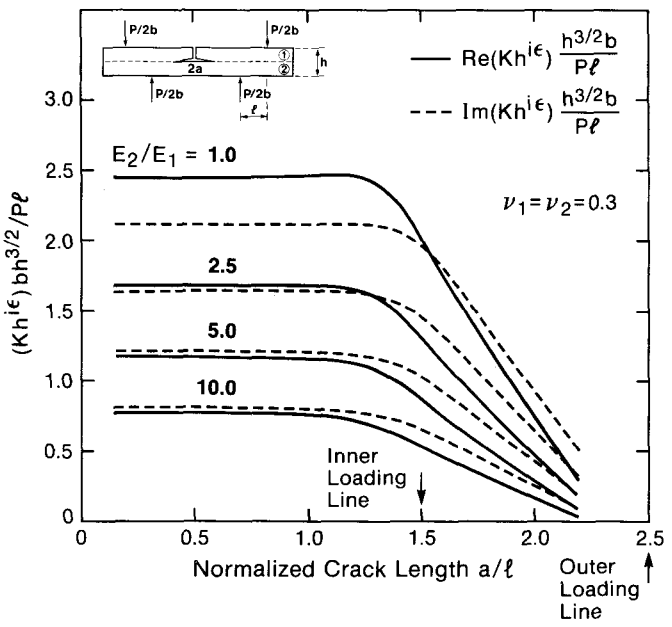

(b)

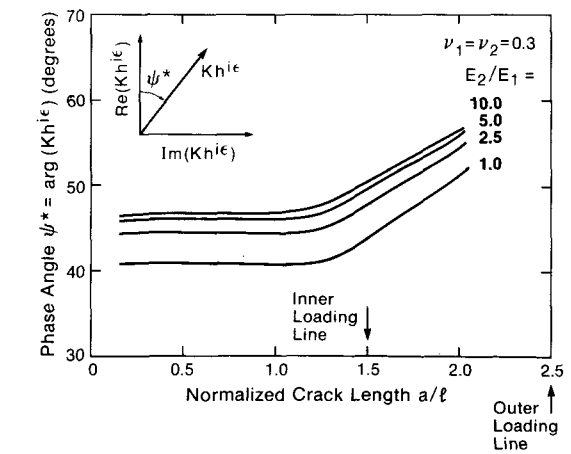

(c)

Fig. 5 (a) The energy release rate with respect to crack length for $h_1/h_2 = 1$; (b) The stress intensity factors and their dependence on crack length for $h_1/h_2 = 1$; (c) The phase angle Ψ^*, with respect to crack length for $h_1/h_2 = 1$.

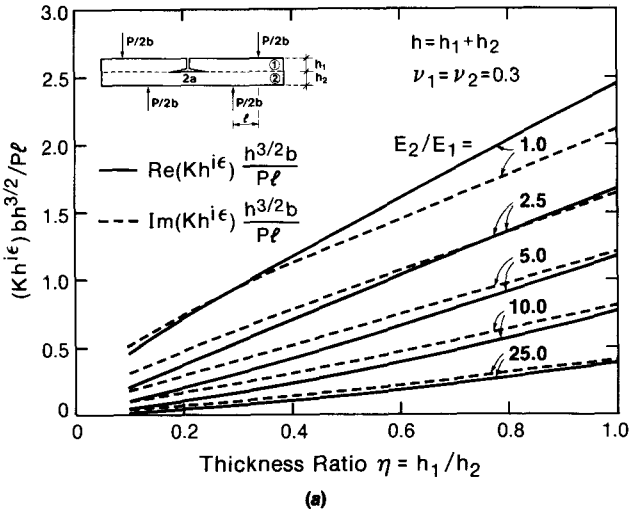

(a)

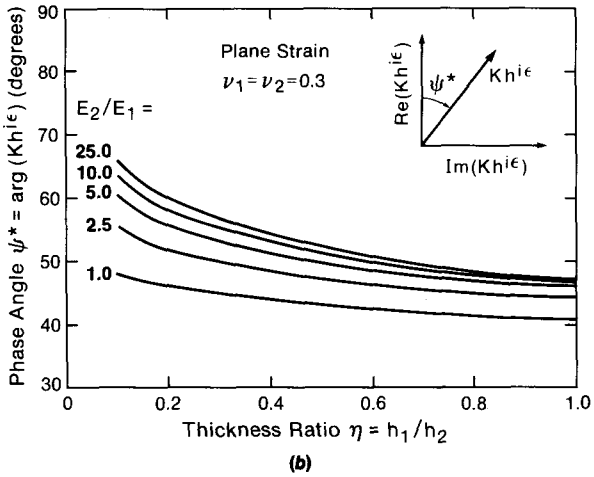

(b)

Fig. 6 (a) Trends in the steady-state real and imaginary stress intensity factors with the thickness ratio and the modulus ratio; (b) The *steady-state* phase angle Ψ^*, with respect to thickness ratio h_1/h_2 and modulus ratio E_2/E_1 for fixed Poisson's ratio, $\nu_1 = \nu_2 = 0.3$

symmetry plane of the order of the smallest thickness of the two layers (Fig. 5(*b*)), and finally decreases linearly with the crack length beyond the inner load line to about zero at the outer supports. Note, also, that the phase angle, ψ^*, of the complex quantity $Kh^{i\epsilon}$ (Fig. 5(*b*)), is relatively insensitive to the modulus ratio in the constant moment region, but varies appreciably as the crack enters the transient moment region.

Within the *steady-state* region, the normalized finite element energy release rates (Fig. 3) are in excellent agreement with the analytical results. The corresponding stress intensities, (Fig. 6) Re $(Kh^{i\epsilon})$ and Im $(Kh^{i\epsilon})$, exhibit trends given by

$$\text{Re}(Kh^{i\epsilon}) = |K|\cos\psi^*$$
$$\text{Im}(Kh^{i\epsilon}) = |K|\sin\psi^* \qquad (13)$$

where $|K|$ is obtained analytically through equations (8) and (12), and the trends in ψ^* with respect to thickness ratio $(\eta = h_1/h_2)$ and modulus ratio are given in Fig. 6(*b*). It is worth noting, however, that for thickness ratios $\eta > 0.6$, the phase angle ψ^* is essentially invariant with modulus ratio. In particular, for beams with one relatively soft material $(E_2/E_1 > 3)$, the phase angle ψ^* deviates very little from 45 deg (Figs. 3 and 6(*b*)). Under these conditions, the phase angle can be set to $\psi^* \approx 45$ deg, for which the components of the complex stress intensity factor take the approximate form,

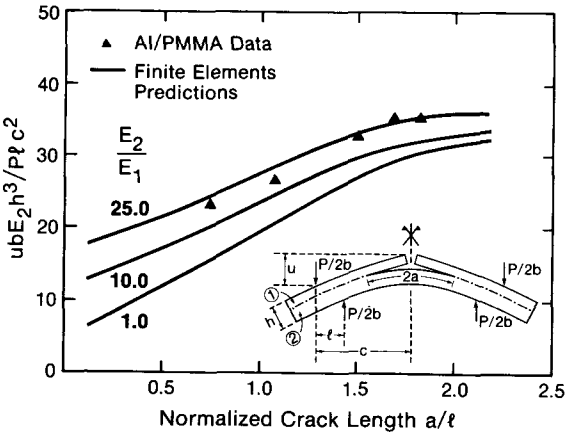

Fig. 7 The relative vertical displacement u of the midpoint of the beam with respect to the outer loading point as a function of the crack length. Also shown are experimental results for Al/PMMA ($E_2/E_1 \approx 25$).

$$\mathrm{Re}(Kh^{i\epsilon}) \simeq \mathrm{Im}\,(Kh^{i\epsilon})$$

$$\simeq \frac{Pl\cosh(\pi\epsilon)}{bh\dfrac{3}{2}\sqrt{1+\lambda}}\left[\frac{3}{2}\left(\frac{1}{\eta_2^3}-\frac{\lambda}{\eta_1^3+\lambda\eta_2^3+\dfrac{3\lambda\eta_1\eta_2}{\eta_1+\lambda\eta_2}}\right)\right]^{1/2} \tag{14}$$

where

$$\eta_i = h_i/h,\ i=1,2.$$

The vertical displacement at the specimen center, u, has also been calculated (Fig. 7) and expressed in terms of the nondimensional parameter, $ub\,E_2h^3/Pl\,c^2$, where $2c$ is spacing between the outer loading points. It is noted that u increases appreciably with increase in crack length, and has the expected linear dependence on a in the region between the inner loading points. This displacement is thus a relatively precise monitor of the crack length and will be used for this purpose in the experimental study (Section 4).

Finally, it is noted that for the material combinations chosen in this investigation, crack surface contact has not been observed even in the smallest element, consistent with the analytical predictions of first contact by Rice (1988). This condition of small scale contact has been used by Rice (1988) to justify the use of K to characterize bimaterial fracture mechanics.

4 Experimental Measurements

4.1 Procedure. An experimental assessment of the utility of the flexure specimen (Fig. 1) for determining interfacial fracture loci has been conducted, using Al/PMMA as a model material couple. Specifically, strips of these materials have been bonded using epoxy, with an initial interface debond created by placing a thin sheet of PTFE along the interface, at the specimen center, prior to bonding. A notch was then introduced through the upper layer, at the center. Erratic interfacial crack propagation from the initial debond, upon loading, was averted by causing controlled extension of the crack prior to testing. This was achieved by placing two thin clamps across the specimen and applying load until crack growth occurred. The clamps arrested the cracks and thus allowed the formation of a well-defined interfacial precrack. Specimen dimensions were selected to allow interface cracking prior to plastic deformation of the Al (Appendix). Suitable dimensions were determined to consist of equidimensional layers, having total thickness > 6 mm.

A displacement transducer was attached to the specimen adjacent to the notch, as needed to measure the vertical displacement, u, upon loading. Loads were imposed in a standard four-point flexure mode, subject to either fixed load or constant load point displacement rate conditions. Typically, with the cracks between the inner loading lines, the cracks extended at a constant rate, subject to constant load, as expected from the constant values of the stress intensities. Crack deceleration occurred when the cracks grew between the inner and outer load lines.

Crack lengths monitored from the displacement measurements were independently checked by means of direct optical observations of the crack front.

Table 2 The results of a typical test conducted at fixed displacement rate on a PMMA/Al specimen

Crack Length a(mm)	$\mathcal{G}_c$ (J/m2)	$\lvert K_c\rvert$ MPa$\sqrt{m}$	ψ (deg)
22.3	11.5	0.25	68
22.6	12.6	0.26	68
25.2	12.7	0.26	68
29.1	12.3	0.26	69
32.5	13.2	0.27	70
35.0	13.3	0.27	71
38.2	12.1	0.26	72
41.0	11.4	0.25	74

To obtain the phase angle, ψ, the units used for all dimensions were meters.

4.2 Results. Compliance measurements performed on specimens with interface cracks having various lengths are initially compared with computed values on Fig. 7. The good correlation in the region between the inner loading points consistent with $E_2/E_1 \approx 25$ for Al/PMMA validates the compliance characteristics of the specimen.[2] Fracture measurements performed using constant displacement rate conditions, with cracks between the inner loading points, reveal that cracks extend at essentially constant load and constant velocity. Consequently, by conducting experiments at different displacement rates and by measuring the load as a function of center point displacement, trends in fracture resistance can be generated by using equation (12) to obtain the critical value of the modulus, $|K_c|$ as well as the phase angle ψ. Results obtained for PMMA/Al using $|K_c|$ and ψ as the characterizing parameters are summarized in Table 2. The results are reproducible between specimens, provided that the bonding conditions are duplicated. The test approach thus seems capable of generating consistent mixed mode interfacial fracture information. The data are also within the general range expected for the Al/PMMA interface ($|K_c| \approx 0.4$ MPa $\sqrt{m}$ for $\psi \approx 0$; Hardwick et al., 1986) but should not be compared directly with the previous data, obtained at $\psi \approx 0$,

[2] Results for crack between the inner and outer loading points are invalid because the loads cause the stress to exceed the yield strength of the Al (Appendix).

because of the differing bonding procedures. A more comprehensive discussion of the crack growth data and the associated interpretation is presented elsewhere (Lund and Evans, 1987).

5 Concluding Remarks

A method for measuring the mixed-mode interfacial fracture resistance of bonded material couples has been devised and analyzed. The utility of the method has been demonstrated by conducting experiments on a model system consisting of PMMA bonded to Al. The results of the test are in a phase angle range typical of many practical interface decohesion problems: notably, thin film decohesion and fiber debonding in composites. The fracture resistance measurements thus have direct applicability to the interpretation and prediction of decohesion phenomena, albeit that scale effects associated with the differing crack geometries would require careful consideration (Rice, 1988).

The present test could also be used in conjunction with other tests to generate fracture loci $|K_c|$ versus ψ, that probe a larger range of phase angles.

Acknowledgment

The authors wish to thank Hibbitt, Karlsson and Sorensen Inc. of Providence, Rhode Island, for the provision of the ABAQUS code used for all the finite element calculations. Financial support was provided by the Defense Advanced Research Projects Agency through the University Research Initiative Program of UCSB under ONR Contract N-00014-86-K-0753.

References

Drory, M. D., Thouless, M. D., and Evans, A. G., 1988, "On The Decohesion of Thin Films," *Acta Met*, Vol. 36, pp. 2019–2028.

Dundurs, J., 1969, Discussion, ASME JOURNAL OF APPLIED MECHANICS, Vol. 36, Series E, pp. 650–652.

Evans, A. G., Rühle, M., Dalgleish, B. J., and Thouless, M. D., 1987, "On Prevalent Whisker Toughening Mechanisms in Ceramics," *Proc. M.R.S. Symposium on Advanced Structural Ceramics*, Vol. 78, pp. 259–271.

Hardwick, D. A., Ahearn, J. S., Desai, A., and Venables, J. D., 1986, "Environmental Durability of Phosphoric Acid Anodized Aluminium Adhesive Joints Protected With Hydration Inhibitors," *J. Mat. Sci.*, Vol. 21, pp. 179–187.

Hsueh, C. H., and Evans, A. G., 1985, "Residual Stresses and Cracking in Metal/Ceramic Systems for Microelectronics Packaging," *Journal of American Ceramic Society*, Vol. 68, No. 3, pp. 120–127.

Kanninen, M. F., and Popelar, 1985, *Advanced Fracture Mechanics*, Oxford University Press, New York.

Lund, J., and Evans, A. G., 1987, "Measurements of Mixed Mode Interfacial Fracture Resistance," to be published.

Matos, P. P. L., McMeeking, R. M., Charalambides, P. G., and Drory, M. D., 1988, "A Method for Calculating K_I^*, K_{II}^* and K_{III}^* in Mixed Mode Bimaterial Fracture," *Int. J. Fract.*, in press.

Parks, D. M., 1974, "A Stiffness Derivative Finite Element Technique for Determination of Elastic Crack Tip Stress Intensity Factors," *Int. J. Fract.*, Vol. 10, pp. 487–502.

Parks, D. M., 1978, "The Virtual Crack Extension Method for Nonlinear Materials Behavior," *Numerical Methods in Fracture Mechanics*, Eds, A. R. Luxmoore and D. R. Owen, eds., pp. 464–478.

Rice, J. R., 1968, "A Path Independent Integral and the Approximate Analysis of Strain Concentration by Notches and Cracks," ASME JOURNAL OF APPLIED MECHANICS, Vol. 35, pp. 379–386.

Rice, J. R., 1988, "Elastic Fracture Mechanics Concepts for Interfacial Cracks," ASME JOURNAL OF APPLIED MECHANICS, Vol. 55, pp. 98–103.

Rice, J. R., and Sih, G. C., 1965, "Plane Problems of Cracks in Dissimilar Media," ASME JOURNAL OF APPLIED MECHANICS, Vol. 32, pp. 418–423.

Rühle, M., Dalgleish, B. J., and Evans, A. G., 1987, "On the Toughening of Ceramics by Whiskers," *Scripta Met.*, Vol. 21, pp. 681–683.

Thouless, M. D., Evans, A. G., Ashby, M. F., and Hutchinson, J. W., 1987, "The Edge Cracking and Spalling of Brittle Plates," *Acta Metall.*, Vol. 35, No. 6, pp. 1333–1341.

APPENDIX

Specimen Design for Crack Growth Before Yield

The limiting elastic load P_y before yielding is given from simple bending theory as;

$$P_y = bh_2^2\sigma_y/3l \tag{A1}$$

where σ_y is the uniaxial yield strength, The critical load P_c for interfacial failure is given in terms of the ratio h_1/h_2 and a critical stress intensity K_c, as;

$$P_c = K_c h^{3/2} b/lA\,(h_1/h_2) \tag{A2}$$

where A is a constant obtained from the finite element solution presented in the text.

To avoid plasticity before crack extension,

$$P_c < P_y, \tag{A3}$$

which gives rise to the inequality,

$$K_c/\sigma_y\sqrt{h_2} < (A/3)\; h_1/h_2(1+h_2)^{3/2}. \tag{A4}$$

The above inequality suggests that, for a given material couple (given K_c and σ_y), plasticity is less likely to occur as the thickness h_2 increases and when $h_1 \approx h_2$.